The Role of Nucleosomes in the Activity of Anti-Cancer Medicine Doxorubicin

Camilleri, Elise

The Role of Nucleosomes in the Activity of Anti-Cancer Medicine Doxorubicin

THESIS

submitted in partial fulfillment of the
requirements for the degree of

MASTER OF SCIENCE
in
PHYSICS

Author :	Elise Camilleri
Student ID :	s3749088
Supervisor :	Prof.dr. J van Noort
Second corrector :	Prof.dr. J.J.C Neefjes

Leiden, The Netherlands, June 25, 2024

The Role of Nucleosomes in the Activity of Anti-Cancer Medicine Doxorubicin

Elise Camilleri

Huygens-Kamerlingh Onnes Laboratory, Leiden University
P.O. Box 9500, 2300 RA Leiden, The Netherlands

June 25, 2024

Abstract

Doxorubicin, an intercalating chemotherapy medication, exerts its effects by interacting with DNA and chromatin structure. Understanding the impact of doxorubicin on the mechanical properties of DNA and chromatin is essential for optimizing its therapeutic efficacy and minimizing side effects. However, the exact mechanisms through which doxorubicin induces these changes remain poorly understood. Here we show that doxorubicin significantly increases the contour length of DNA and induces a shift in the linking number towards negative values, as it causes DNA to untwist. Gel electrophoresis results further demonstrate histone dissociation in chromatin samples treated with doxorubicin, highlighting its disruptive effect on chromatin structure. Our findings underscore the critical importance of understanding drug-DNA interactions at the molecular level. By studying how doxorubicin modifies DNA and chromatin structure, we contribute to advancing scientific understanding and pave the way for the development of improved chemotherapeutic agents tailored to more effectively target cancer cells.

Contents

Chapter 1

Introduction

Doxorubicin is one of the most effective chemotherapy drugs available today [1]. However, despite its widespread use, the exact mechanisms by which doxorubicin targets cancer cells and its selective toxicity remain a topic of debate within the scientific community. Studies have shown that doxorubicin intercalates into DNA, causing changes in the chromatin structure and preventing the replication of rapidly dividing cells [2]. Furthermore, DNA intercalating drugs are known to increase the distance between DNA base pairs and reduce the helical twist by an angle specific to the intercalating molecule [3].

Magnetic tweezer experiments have been used to study intercalating drug activities at a molecular level, demonstrating that the topology of the DNA plays a critical role in regulating the initiation of transcription, a process essential for the regulation of cell division [4]. As a result, a thorough understanding of the DNA structure and how doxorubicin modifies its mechanical properties is fundamental to advancing cancer treatment.

DNA is a negatively charged molecule consisting of two polynucleotide chains held together by hydrogen bonds between complementary nucleotides [5]. Each strand of the DNA helix twists in a right-handed spiral, with ten nucleotides composing one complete turn. These nucleotides are covalently linked together to form a stable backbone structure. In eukaryotes, DNA is wrapped around positively charged histone proteins, and the compact structure of 145 base pairs (bp) of DNA wrapped around an octamer of histones is called a nucleosome [6]. Nucleosomes, in turn, stack onto each other to form tightly packed structures called chromatin.

The arrangement of DNA around histone proteins forming the chromatin, not only compacts the DNA allowing it to fit into the microscopic space of the nucleus, but also plays an important role in regulating gene expression [7]. The dynamic structure of chromatin allows for the controlled access to genetic information, which is essential for various processes such as DNA transcription, replication and repair.

Cancer cells differ from normal healthy cells by replicating at a significantly faster rate. The uncontrolled growth and accelerated rate of cell division implies a disruption of the chromatin structure at a larger scale, as chromatin is in a more open and accessible state to facilitate DNA replication [8]. During DNA replication, chromatin unwinds, and nucleosomes are partially disassembled, creating opportunities for doxorubicin to intercalate into the exposed DNA. We hypothesise that the chemotherapy drug doxorubicin works by exploiting this vulnerability, intercalating into the accessible DNA and disrupting cancer cells' cellular processes. Doxorubicin may be more effective against rapidly replicating cancer cells due to the increased presence of bare DNA, or it may cause nucleosome dissociation itself, further enhancing its therapeutic efficacy.

Throughout this research project, I conducted pulling and twisting experiments with bare DNA in the absence and presence of clinically relevant 5 μM doxorubicin using magnetic tweezers to observe doxorubicin's interactions [9] [10]. Pulling experiments were then repeated with chromatin to compare results as well as gel electrophoresis experiments. My result supports the hypothesis that doxorubicin intercalation causes chromatin to become less stable, leading to histone dissociation and the creation of bare DNA.

By investigating these aspects, my thesis aims to contribute to a deeper understanding of doxorubicin's mechanisms, ultimately aiding in the development of better cancer treatments.

Chapter 2

Theoretical Context

By analysing the structural and mechanical changes of DNA and chromatin before and after the addition of doxorubicin, valuable information can be obtained such as the number of doxorubicin molecules intercalated and how it affects the mechanical properties of DNA. Understanding how the extension of DNA and chromatin changes with applied force is crucial when using single-molecule force spectroscopy techniques to quantify the effects of doxorubicin.

2.1 Magnetic tweezers

Magnetic tweezers were used to manipulate a magnetic bead attached to DNA or chromatin. The setup involved DNA or chromatin labeled with digoxigenin on one end, which was tethered to an anti-digoxigenin coated surface. The opposite end of the DNA or chromatin was labeled with biotin, allowing it to bind to streptavidin on a magnetic bead. A force is then exerted on the molecule by using a magnet which exerts a magnetic field on the bead. The magnet position can be changed by using a motor so as to twist or pull on the tethered bead. As the magnet position goes down, the force exerted on the bead is increased, causing the bead (attached to the DNA/chromatin) to increase in height as it is pulled up.

The force increases exponentially as the magnet approaches the bead, according to the equation

$$F = F_{max} \cdot (0.7e^{-\frac{h}{L_1}} + 0.3e^{-\frac{h}{L_2}}) + F_0 \tag{2.1}$$

Where h is the bead height, L_1 and L_2 are two decay lengths that describe

the magnetic field, 1.4 mm and 1.8 mm respectively, F_0 is 0.01 pN, and F_{max} is 85 pN when 2.8 μm beads are used, as is the case in this thesis [11].

The exponential relationship shows the sensitivity of the magnetic tweezers used as small changes in the magnet position result in significant changes in the applied force allowing for manipulation of DNA and chromatin allowing for measurements done in the nm range.

2.2 Worm-like chain model

The elastic behavior of DNA in response to a pulling force can be described using the worm-like chain (WLC) model. This model considers DNA to be a flexible rod characterized by the contour length L, and a measure of its stiffness [12]. Each base pair adds 0.34 nm to the contour length [13]. The length scale that defines the stiffness is called the persistence length A, which describes the distance over which the chain maintains its directional orientation. Beyond this distance, thermal fluctuations cause the chain direction to become random. Given a unit tangent vector $\hat{t}$, a correlation function for the orientation of the polymer can be defined as

$$\langle \hat{t}(0)\, \hat{t}(L) \rangle = \langle cos(\theta) \rangle = e^{\frac{-l}{A}} \tag{2.2}$$

where θ is the angle between the polymer and $\hat{t}$, and l is the distance between 2 segments along the contour of the chain [14]. Thus, the correlation between the orientations of two polymer segments decreases exponentially with the distance between the segments.

The higher the value for A the less flexible the polymer is. For double-stranded DNA, A is $40-55$ nm [15]. Using the WLC model, the response of DNA to applied forces (f) can be described as

$$z = L(1 - \frac{1}{2}\sqrt{\frac{k_B\, T}{F\, A}} + \frac{F}{S}), \tag{2.3}$$

where z is the extension of DNA, and k_B, T and S are the Boltzmann constant, temperature and stretch modulus respectively.

Figure 2.1 shows a force-extension curve obtained from magnetic tweezer pulling measurements on 7.9 kbp DNA. The data points are fit with the WLC model, which accurately captures the behavior of the DNA molecule

under tension, showing the expected persistence length of 45 nm and contour length of 2.71 μm. As can be seen from the figure, the extension of DNA in response to force does not increase linearly due to the WLC behavior. Instead, DNA initially extends easily with small applied forces, but as the force increases and the DNA approaches its contour length, much greater forces are required for further extension.

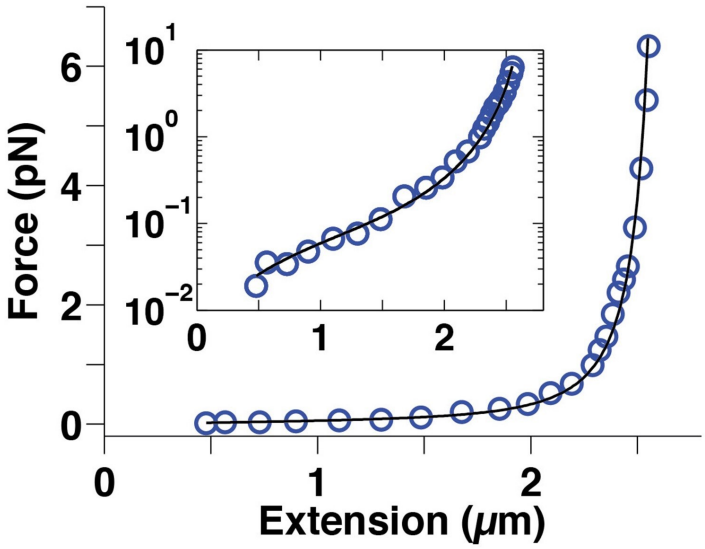

Figure 2.1: Force extension graphs for DNA. *Circles denote the experimental data obtained from magnetic tweezer measurements while the solid black line shows the WLC fit having contour length 2.71 μm and a persistence length of 45 nm taken from [13]*

2.3 DNA linking number

The theory of DNA supercoiling describes the behaviour of torsionally constrained DNA by keeping track of changes in the linking number Lk. The linking number is the number of times a molecule twists around its own helical axis [16] [17]. This two-fold rotation axis of DNA is shown in Figure 2.2 (a). DNA supercoiling plays a crucial role in the compact packaging of genetic material within cells. Supercoiling of DNA condenses the DNA structure into chromatin, thereby facilitating its packaging. In eukaryotic cells, this process is achieved by wrapping DNA by negative supercoiling around histone proteins which reduces the linking number

relative to free DNA (Figure 2.2 (b)).

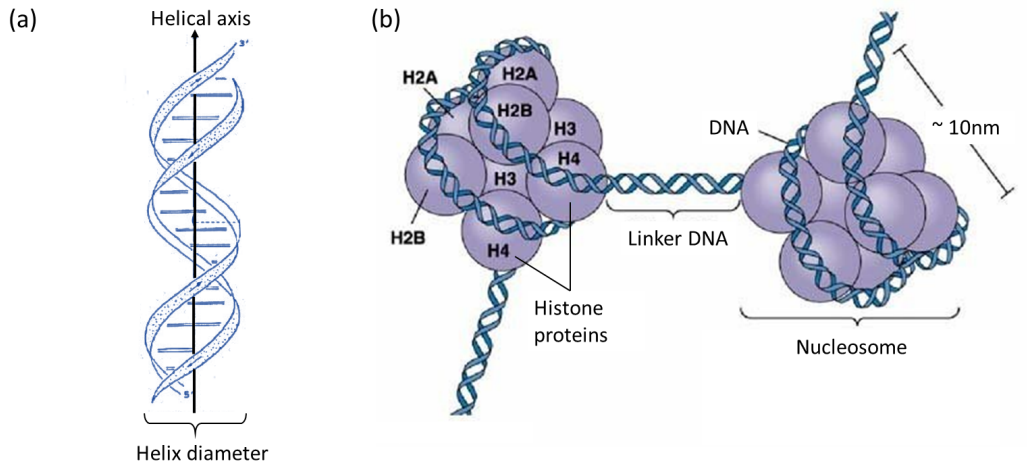

Figure 2.2: DNA and nucleosome structures *(a) Schematic of the DNA structure taken from [18] showing the twisting of DNA around its helical axis. In eukaryotes the DNA is found wrapped around histone proteins as shown in (b) taken from [19]. The schematic shows negative supercoiling of DNA which decreases the linking number relative to free DNA.*

When the DNA is not subjected to any torque the linking number is referred to as Lk_o which depends on the number of base pairs according to

$$Lk_o = \frac{n_{bp}}{\gamma}. \tag{2.4}$$

γ defines the number of base pairs per helical turn of a DNA molecule [20]. For relaxed, B-form DNA, this value, as extracted from crystal structures, is typically taken to be 10.5 base pairs per helical turn [21]. When the DNA structure is distorted, this value can change as the linking number is altered.

To manipulate the linking number of DNA using the magnetic tweezers, DNA labelled with multiple biotin and digoxigenin attached to a magnetic bead is rotated to introduce supercoiling into the DNA. Its linking number is hence changed by adding positive or negative turns. Figure 2.3 shows the extension vs. linking number for 7.9 kbp DNA at constant forces taken from [13]. At forces of 0.5 pN and below, the graphs are symmetric, indicating that the direction of magnet rotation does not significantly impact plectoneme formation. However, as the force increases, asymmetry

is introduced because the chirality of DNA starts to have an effect. For positive rotations of the magnet, supercoils form, and the DNA strand extension decreases. In the case of negative twist, DNA melting of the two strands occurs, causing some twist in the double helix to be lost. This leads to a "flat ladder" configuration where the two strands come apart, resulting in a gain in extension. Consequently, an equilibrium is established where some base pairs may melt, extending in length but containing no twist, as the DNA is undertwisted.

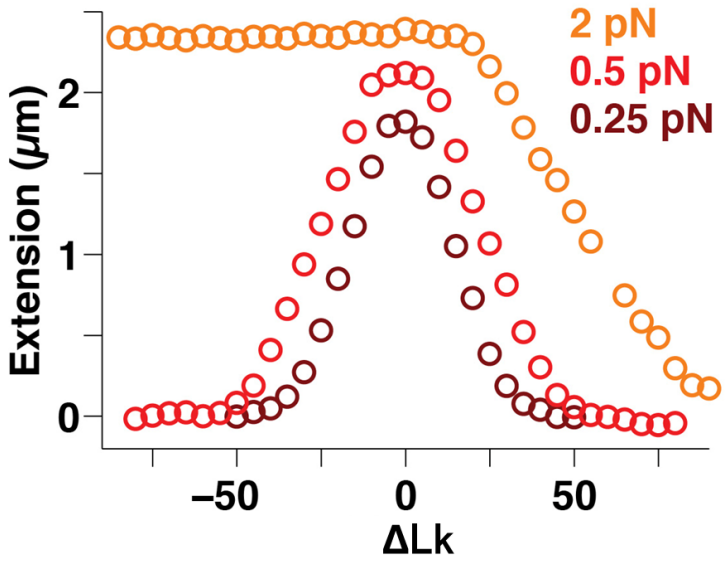

Figure 2.3: Extension vs change in linking number for DNA. *Circles denote the experimental data obtained from magnetic tweezer measurements at forces of 0.25 pN, 0.5 pN and 2 pN on a 7.9 kbp DNA taken from [13]*

Intercalating drugs insert themselves between two DNA base pairs, increasing the contour length, and affecting the persistence length and the linking number [22]. The DNA base pairs, which form the helical staircase, are hydrophobic and stack tightly, leaving no water in between [23]. To accommodate the hydrophobic doxorubicin molecules, the overall helix structure must untwist slightly to make space.

In this research project, doxorubucin's effect on Lk was quantified by studying the change in linking number (ΔLk_o). The number of doxorubicin molecules intercalated in the DNA strand (n_{DOX}) is directly related to

the change in linking number as each doxorubicin molecule adds ΔLk_{DOX}:

$$\Delta Lk_o = n_{DOX} \cdot \Delta Lk_{DOX}. \tag{2.5}$$

When doxorubicin intercalates and reduces the linking number, it can affect chromatin unfolding by altering the torsional stress within the DNA, potentially making nucleosome unwrapping more favorable. As a result, understanding how chromatin unfolds is important for understanding the effects of intercalating drugs like doxorubicin.

2.4 Unfolding steps of chromatin

Chromatin consists of nucleosomes, which include about 145-147 base pairs (bp) of DNA wrapped around a histone octamer. The distance between the centers of adjacent nucleosomes is referred to as the nucleosome repeat length (NRL), and is hence 145-147 bp plus the length of the linker DNA [24].

Typically when a chromatin fiber is subjected to a pulling force, it unfolds in four distinct steps, as illustrated in Figure 2.4 (a). Initially, at forces below 4 pN, the nucleosomes in chromatin are predominantly stacked on top of each other, and are hence in the conformation marked as structure I. In this state, the chromatin is stretched without breaking DNA-histone or nucleosome-nucleosome interactions. As the force increases, a transition to structure II occurs, resulting in the partial unwrapping of nucleosomes. Around 4-5 pN, a significant gain in length is observed due to the unstacking of nucleosomes. At forces up to 10 pN, the nucleosomes continue to unwrap, transitioning to structure III, characterized by a singly wrapped nucleosome. Complete unwrapping happens at forces above 40 pN, leading to structure IV, where the fully unwrapped chromatin behaves according to the worm-like chain (WLC) model of bare DNA.

The transitions from structure I to II and from structure II to III are gradual and occur in equilibrium, meaning that chromatin constantly folds and unfolds. This results in a fluctuating extension rather than discrete steps. However, between forces of 10-40 pN, discrete steps of approximately 25 nm are observed in the force-extension curve. These steps represent the sequential unwrapping of DNA from the histone octamers in the nucleosomes and can be observed when performing single molecule

force measurements on chromatin as can be seen in the force-extension curves of a chromatin fiber shown in Figure 2.4 (b). The observed discrete steps in the force-extension curve directly indicate the step-by-step release of DNA from histones as the tension increases were each complete unwrapping step releases approximately 77 bp.

Figure 2.4 (c) shows force extension curves at low force for three chromatin fibers having different nucleosome repeat length (NRL). Regardless of the NRL, a plateau is observed at a low force showing a gain in length as the nucleosomes unstack and begin to unwrap.

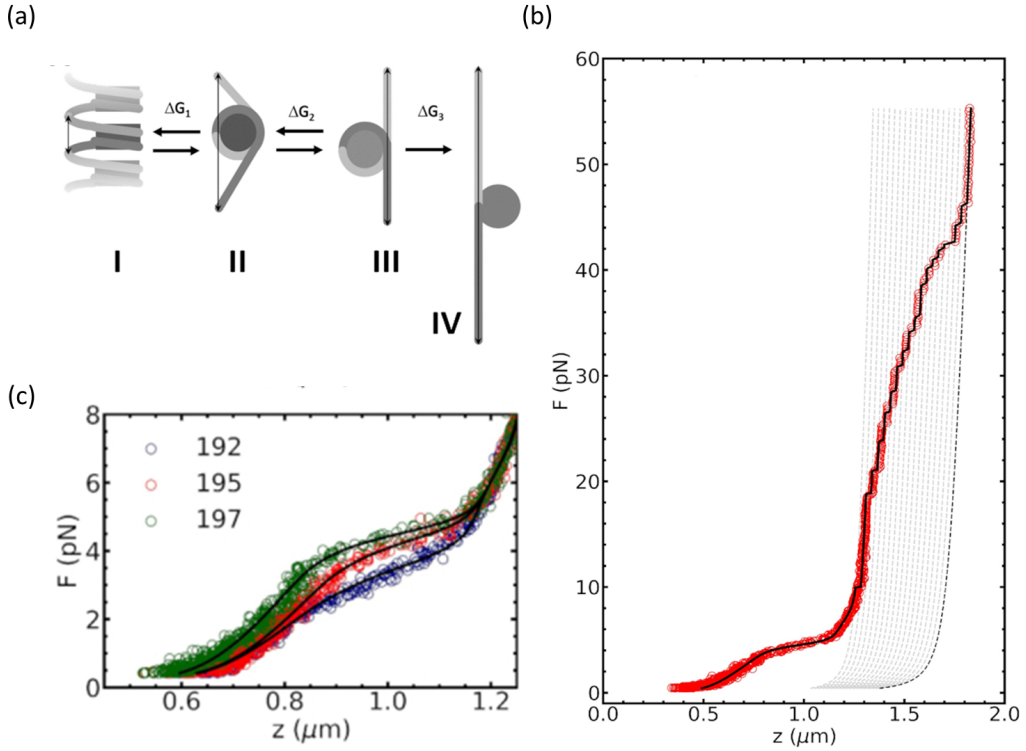

Figure 2.4: Single molecule force spectroscopy experiment results showing force extension curves of Chromatin *taken from [25] (a) schematic showing chromatin unfolding steps; I represents unstacking of the nucelosomes, II partial unwrapping, III unwrapping to a tetrasome, IV histone dissociation and transition to bare DNA. (b) Force extension graph for chromatin, a statistical mechanics model was fitted to the raw data showing 18 nucleosomes,* $\Delta G_1 = 23 \pm 1 k_B T$ *and* $\Delta G_2 = 8 \pm 1 k_B T$*. (c) Force extension curves for pulling forces up to 8 pN on 3 chromatin fibres having nucleosome repeat length (NRL) 192, 197 and 195. A plateau is seen for all 3 chromatin fibres between 3−5 pN*

Chapter 3

Materials and Methods

3.1 DNA preparation

All DNA twisting and pulling experiments were conducted using DNA made from the plasmids containing repetitions of the 601 DNA fragment, a 147 base pair (bp) double-stranded DNA fragment with high affinity for histone octamers. The use of this sequence was important as it ensured uniformity in the base-pair sequence of all DNA strands and facilitated precise chromatin reconstitution by having predefined nucleosome positions.

3.1.1 DNA multi-labeling

A plasmid containing 15x 601 core sequences flanked by 50 base pairs of identical linker DNA was chosen. Multi-biotin handles and multi-DIG handles were prepared using polymerase chain reaction (PCR), and the PCR product was purified using the Wizard gel and PCR purification kit. The plasmid DNA was digested in a single tube using the BsaI restriction enzyme to generate cohesive ends compatible with hairpin oligonucleotides. Hairpins were designed with one strand biotinylated and the other labeled with digoxigenin, featuring a BsaI-compatible overhang for subsequent ligation to nucleosome DNA. The hairpins were annealed by heating to 95°C for 2 minutes, followed by cycling from 94°C, decreasing 1.6°C per cycle with a 0.1°C ramp-down, for a total of 46 cycles. Subsequently, the hairpins were ligated using T4 DNA ligase, and T5 Exonuclease treatment was used to remove unligated hairpins. The DNA contour length relevant for our experiments, the number of base pairs between the biotin and digoxigenin labels, was 4531 bp.

3.1.2 DNA mono-labelling

Another DNA sample using a plasmid contatining 16 repeats of the 601 fragment was then prepared and mono-labeled with biotin and digoxigenin. Due to the mono-labeling, this DNA could only be used for pulling experiments and was later used for chromatin reconstitution. The plasmid containing 16x 601 core sequences was flanked by 50 base pairs of identical linker DNA was chosen. The plasmid DNA was digested using the BsaI restriction enzyme to generate cohesive ends compatible with hairpin oligonucleotides. These hairpins were designed similarly, with one strand biotinylated and the other labeled with digoxigenin. To prepare the hairpins, denaturation was achieved by heating to 95°C for 2 minutes, followed by annealing through cycling from 94°C, decreasing 1.6°C per cycle with a 0.1°C ramp-down, for a total of 46 cycles. The hairpins were then ligated using T4 DNA ligase, and T5 Exonuclease treatment was used to remove unligated hairpins. The final contour length of this DNA was 3152 bp.

3.2 Chromatin reconstitution

Chromatin was reconstituted from DNA and histones using the process of salt dialysis. Salt dialysis involves mixing bare DNA, prepared as explained in Section 3.1.2, with histone octamers in a buffer with a high salt concentration. The salt concentration was then gradually reduced to facilitate nucleosome formation. Four DNA:histone titrations were performed (1:0.9, 1:1.4, 1:1.9, and 1:2.4) to determine the optimal ratio for chromatin reconstitution.

3.2.1 Preparation of buffers

A solution of 50x TE buffer (pH 7.5) was prepared by combining 0.5 M Tris(hydroxymethyl)aminomethane (Tris) hydrochloride (Invitrogen, 15504-020) and 50 mM ethylenediaminetetraacetic acid (EDTA, Sigma-Aldrich, 60-00-4 EDS). This buffer was then diluted to 1x TE using Milli-Q water, stored at 4°C, and allowed to cool before use. Next, a high salt buffer was prepared, consisting of 2 M sodium chloride (NaCl, Honeywell, 59888) and 1x TE. Three separate 10,000 MWCO dialysis membranes (Thermo Scientific, 69572) were placed upright on a floater and inserted into the high salt buffer to soak for at least 15 minutes.

3.2.2 DNA-histone titrations

Four titrations with different DNA-to-histone ratios were prepared in separate protein low-binding tubes. Each titration contained a high salt buffer made by combining 2 M NaCl and 1x TE, DNA mono-labeled with digoxigenin and biotin prepared as described in section 3.1.2, and histone octamer (EpiCypher). The final concentration of DNA was 0.02 μg/μL for each of the four titrations, and the amount of histone used was determined to achieve molar ratios of 1:0.9, 1:1.4, 1:1.9, and 1:2.4 (DNA:histone), respectively. Additionally, a final concentration of 0.0038 μg/μL of competitor DNA having length 147 bp was added to each tube to act as a buffer, preventing excess histones from remaining in solution after reconstitution. The final volume of each titration was adjusted to 50 μL using the high salt buffer.

These titrations were then carefully transferred into the pre-soaked dialysis membranes.

3.2.3 Salt dialysis

The assembly containing the three dialysis membranes with DNA-histone titrations on a floater in a beaker containing high salt buffer was taken to a cold room and connected to a pump, as shown in Figure 3.1. A low salt buffer of 1x TE at 4°C was also attached to the pump according to the schematic in Figure 3.1.

A stirrer was added to the beaker containing the membranes to ensure continuous mixing and the flow rate was set to 0.9 mL/min ensuring that the salt concentration was reduced at a slow and controlled rate for proper assembly of chromatin. The volume in the beaker was maintained by pumping an equal volume of low salt buffer into the beaker as high salt buffer was pumped out. Initially, as the salt concentration begins to reduce, the $(H3\text{-}H4)_2$ tetrasomes begin to assemble first on the 601 regions of the DNA. This is followed by the binding of the H2A and H2B histone dimers at a lower salt concentration [26].

This setup was maintained overnight in the cold room, and the pump was stopped after 90% of low salt buffer had been pumped through and the solutions from the dialysis membranes were collected into individual low-binding tubes. The final volume collected from each dialysis membrane was observed to be 65 μL, larger than the initial 50 μL. The reconsti-

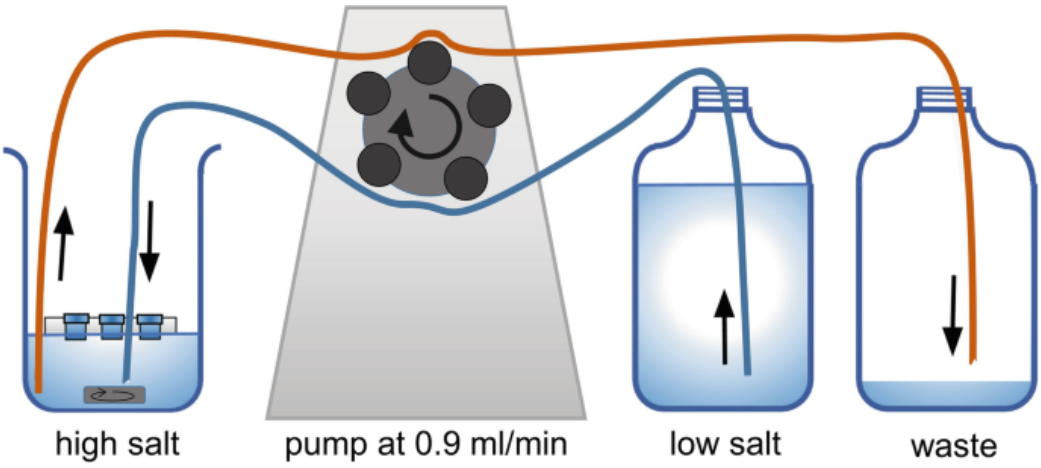

Figure 3.1: Schematic showing salt dialysis assembly. *The DNA - histone titrations are placed on a floater in high salt buffer. Low salt was pumped in and solution from the beaker containing the titrations was flowed out at a constant flow rate of 0.9 mL/min into a waste jar. (Figure taken from [26])*

tuted chromatin was stored at 4°C.

3.2.4 Gel electrophoresis

Gel electrophoresis was then conducted to assess the efficiency and stability of chromatin reconstitution. A 1.2% agarose gel was prepared in 0.2X Tris-Boric acid (TB) buffer. To make 0.2X TB buffer, Tris and boric acid were dissolved in deionized water making a stock solution of 5X TB which was then diluted with deionized water to achieve the desired concentration. The agarose gel was cast in a mold containing a comb which forms the shape of the wells and once solidified it was transferred in an electrophoresis chamber.

To prepare the samples for gel electrophoresis, solutions with the following final concentrations were made separately: 0.48X DNA ladder (Thermo Scientific, SMO331), 0.189 μg/μL mono-labeled DNA, and 12 ng/μL reconstituted chromatin samples with DNA-to-histone molar ratios of 1:0.9, 1:1.4, 1:1.9, and 1:2.4. Equal amounts of 3% glycerol and 0.24X Safe Red dye were added to each solution. Nuclease free water was added as needed to ensure a final volume of 12.5 μL per solution. Glycerol was added to increase the density of the samples, ensuring they remained in place during the run and did not diffuse into the surrounding TB buffer. Meanwhile,

Safe Red dye was added to visualize the bands.

The prepared solutions were then loaded into separate wells in the agarose gel. The gel was run in 0.2X TB buffer at a voltage of 150 V until the dye front had migrated an appropriate distance.

After ensuring that the chromatin was successfully reconstituted, another agarose gel was prepared to investigate the impact of doxorubicin on chromatin. A concentration of 5 μM doxorubicin was added to each of the reconstituted chromatin samples, as well as to bare DNA, all having final concentrations of 11 ng/μL. The samples were allowed to incubate for 10 minutes. Following the incubation, solutions of 0.48X DNA ladder, 11 ng/μL bare DNA, and 11 ng/μL chromatin made from DNA molar ratio 1:1.9 were prepared. Equal amounts of 3% glycerol and 0.24X Safe Red dye were added to each of the 8 solutions. Nuclease free water was added as necessary to ensure a final volume of 14.5 μL per tube.

The prepared contents were then loaded into separate wells of the agarose gel. The gel was run in 0.2X TB buffer at a voltage of 150 V until the dye front had migrated an appropriate distance.

3.3 Magnetic tweezer experiments

3.3.1 Preparation of buffers

To prepare the sodium borate (SB) buffer, we mixed the following components to achieve their final concentrations: 10 mM Tris- HCl(pH 7.5), 150 mM NaCl, 1 mM EDTA (pH 8), 1 mM Dithiothreitol (DTT), 3% glycerol, and 100 μg/mL Bovine Serum Albumin (BSA). For the chromatin buffer, we combined 10 mM HEPES (pH 7.6), 100 mM NaCl, 2 mM $MgCl_2$, 0.1% Tween-20, and 2 μg/mL Bovine Serum Albumin (BSA). SB buffer was used for flow cells containing DNA, while chromatin buffer was used for flow cells containing chromatin. PPB buffer was made by mixing 0.02% pluronic F127 into 100 ml 1x PBS buffer. The solution was stored at 4°C.

Blotting grade buffer (BGB) was prepared by adding 60 mg/mL of blotting grade blocker (Bio-Rad, non-fat dry milk) to 40 mL of SB buffer. The mixture was rotated at 4°C overnight. Following rotation, the mixture was ultracentrifuged at 35,000 rpm for 30 minutes. The supernatant was then filtered using a 0.2 μm filter. The protein concentration of the filtered su-

pernatant was measured using the Invitrogen protein kit (Q33211) on a Qubit fluorometer. Finally, the BGB buffer was diluted with SB buffer to a final concentration of 4 mg/mL.

3.3.2 Bead preparation

Covalently coupled streptavidin beads (Dynabeads M-280, Thermo Fisher) were kept at 4°C in a solution of phosphate-buffered saline (PBS) with 0.02% NaN_3 (pH 7.4). The superparamagnetic and hydrophobic Dynabeads M-280 have a diameter of 2.8 μm. Before use, they were washed three times with PBS. During the washing process, the beads were separated from the liquid using a magnetic stand, the supernatant was discarded, and they were resuspended in fresh PBS each time. Following the last wash, the beads were resuspended in a solution of PBS and 2 mg/mL recombinant bovine serum albumin (BSA) and then passivated for 10 minutes on a rotator to block any open binding sites. After the passivation, the solution was discarded, and the beads were resuspended in SB or chromatin buffer to achieve a final concentration of 0.01 μg/μL.

3.3.3 Flow cell preparation

The flow cells were made using a 0.1% nitrocellulose-covered glass slide and coverslip with three channels in between (Figure 3.2). All equipment used to make the flow cells, including the metal stamp and precision pointer tweezers used to form the parafilm channels, were washed with 70% ethanol and milli Q water before use ensuring sterility as well as to minimise any background noise. After using the metal stamp to cut the channels out of the parafilm, the parafilm was placed between a glass slide and a coverslip. The assembly was then heated to melt the parafilm, forming three leakproof channels. For each sample preparation, the same condition was repeated three times to ensure the replication of results.

After flow cells were assembled, a final concentration of 2 μg/mL anti-digoxigenin (Anti- Dig) antibody in sodium borate (SB) buffer was inserted in each channel and allowed to incubate for 10 minutes. This was followed by the addition of 4 mg/mL blotting grade (BGB) buffer and a minimum incubation time of 3 hours at room temperature. During this waiting period, it was ensured that the sample did not dry up by adding PBS droplets on the flow cell inlets and outlets.

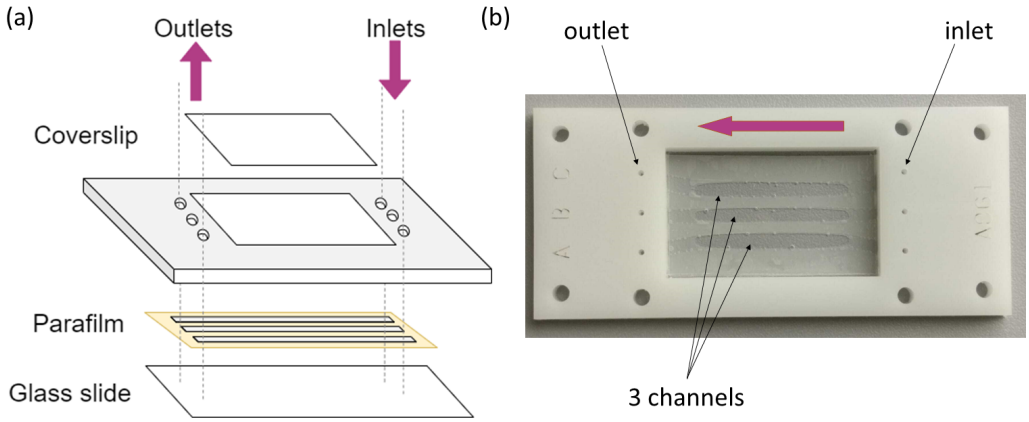

Figure 3.2: Flow cell assembly *(a) Schematic showing the different components making up the flow cell. The parafilm with 3 channel cut outs was placed between a coverslip and glass slide. The setup was then heated to melt the parafilm and make 3 leakproof channels. (b) Image of the flow cells used with the glass slide having dimensions 24 x 60 mm and the coverslip 24 x 40 mm.*

After the incubation period, the channels were washed once with SB or chromatin buffer, then DNA or chromatin was added. A final concentration of 0.002 ng/μL was used for bare DNA experiments while for chromatin experiments the final concentration was that of 0.005 ng/μL. Ten minutes after, the channels were washed once more with SB or chromatin buffer and the 0.1 μg/μL passivated Dynabeads M-280 were added to each channel followed by an incubation time of 10 minutes. The final step of the flow cell preparation involved washing the channels with 0.1 mg/ml BSA in PPB buffer.

3.3.4 Measurement procedure

The magnetic tweezer setup used to carry out pulling as well as twisting measurements on both chromatin and DNA, has been described by Kruithof et al. [11]. After mounting the flow cells on the magnetic tweezers they were allowed to acclimatize for a few minutes to reduce thermal drift. Graphs (a) and (b) in figure 3.3 show the magnet position during pulling or magnet rotation during twisting measurements on bare DNA respectively. Graph (a) shows that for each pulling measurement, the magnet moved towards the flow cell. Conversion from shift to force exerted was done using equation 2.1. As the magnet shift decreased, the force increased from 0 to 60 pN in 10 seconds, followed by a waiting time of 1 s.

The magnet was then pulled away, the shift increased and the force was decreased back to 0 pN with a ramp time of a further 10 s. This was repeated twice with a start and end delay of 1 s.

In the case of chromatin pulling, the magnet followed a similar trajectory to that of pulling on bare DNA (Graph (a) in figure 3.3). However, lower forces were used to ensure that histones do not dissociate from the chromatin. A series of pulling experiments were done with the force increasing from 0.1 pN to 8 pN. At the end of the experiments, the beads were subjected to pulling forces ranging from 0.1 pN to 60 pN to infer the number of nucleosomes and tetrasomes present from the resulting force-extension curves.

In the case of twisting, the magnetic tweezer settings were changed to rotation with a starting position of 0 turns following the trajectory shown in figure (c). After an 8-second delay, the magnet rotated at a rate of 1.7 rotations/ second for 30 seconds, counter rotated at the same rate for the 60 seconds following, and then returned to the starting position. Twisting measurements were done at a force of 0.3 pN, 0.7 pN, 0.9 pN and 1.1 pN.

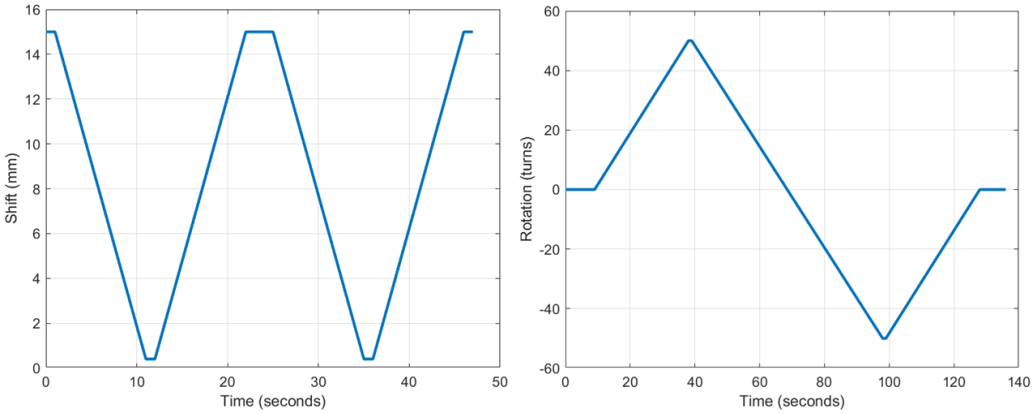

Figure 3.3: Trajectory of magnetic tweezer motor *when (a) pulling and (b) twisting bare DNA.*

Doxorubucin was then injected into the flow cells at a final concentra-

tion of 5 μM followed by an incubation time of 10 minutes. Pulling and twisting measurements at different forces were then repeated.

3.4 Data Analysis

3.4.1 Drift correction

First, any drift present in the measurements was corrected. This was done by fitting an exponential decay model to selected data points. For pulling experiments, data points were selected when the force was low, with the bead pushing on the surface. To achieve this, the top 10% of the shift data was chosen for drift correction. For twisting experiments, the top 10% of the rotation data was selected to ensure that only the maximum positive rotations were considered. When rotating DNA, it was also important to select data when the beads were at their lowest, corresponding to a high number of plectonemes. At a force of 1 pN or higher, only positive plectonemes form, so selecting the top 10% of the rotation data accounted for this.

After selecting the data, initial values were supplied for the exponential decay fit, which included parameters for the time constant of the exponential decay (assumed to be infinite for fitting a straight line with a slope), the offset (the level the drift would stabilize at as time approaches infinity), and the amplitude (the value at $t = 0$) which was taken as the median of the selected data.

3.4.2 Correcting for bead tethering offset

In an ideal case scenario, the DNA is attached to the superparamagnetic bead at the south pole. However, in the case that the DNA is not attached at the south pole, part of the DNA height (denoted as z_{bead} in Figure 3.4 (b)) is hidden and needs to be accounted for. This was done by examining the trajectory in the xy-plane of the bead. When $z_{bead} = 0$, the measured height h_m is equal to z_{max} (Figure 3.4 (b)). However for $z_{bead} > 0$, the xy fluctuations of the bead lie within a circular annulus as shown in Figure 3.4 (c). A nonlinear least squares method in Python was then implemented to fit a circle to the data points obtained, determining the estimated center and radius of the circle that best fits the data points.

Using simple trigonometry, the radius of the trajectory followed by the bead (X_{bead}) in the xy-plane can be related to h_2 since

$$a = \sqrt{R_{bead}^2 - X_{bead}^2} \tag{3.1}$$

whereby $z_{bead} = R_{bead} - a$. Taking this into account, the corrected extension of the DNA is defined as

$$z_{max} = z_{bead} + h_m \tag{3.2}$$

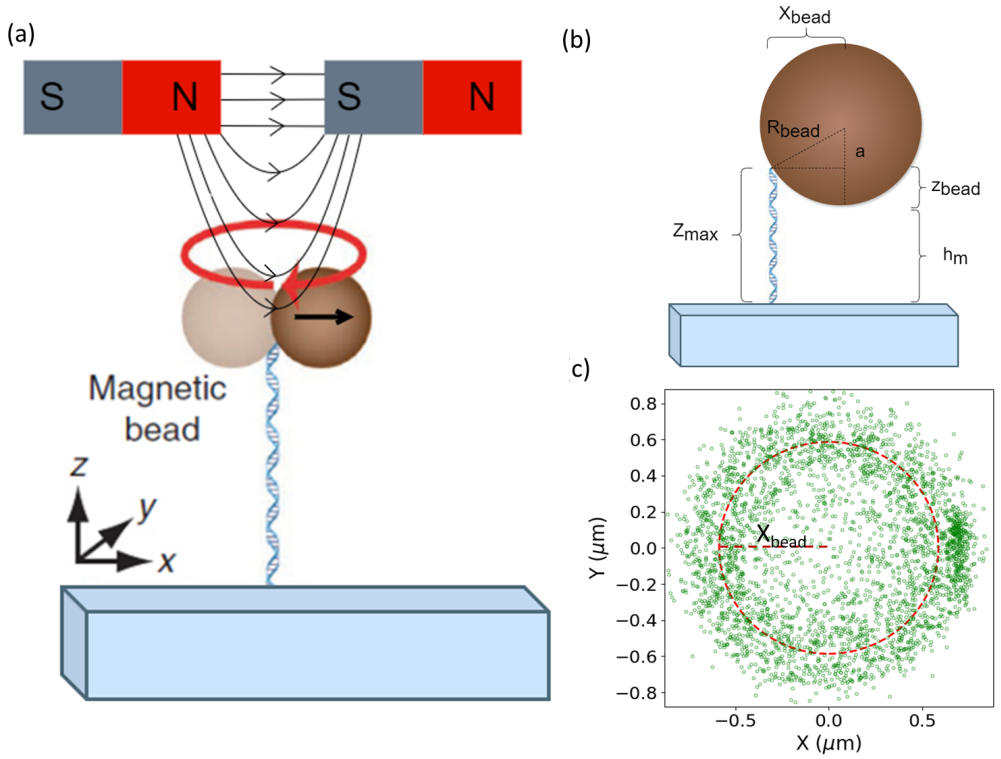

Figure 3.4: Fixing the offset due to DNA tether to the bead *(a) Diagram adapted from [13] showing the bead attached to DNA held in place due to the magnetic field exerted by two magnets in the magnetic tweezer setup. (b) Diagram showing components needed to be measured to determine the offset (z_{bead}) (c) Graph showing x and y position of bead for one DNA strand. Data points are shown in green, red circle shows least squares fitting done on the data obtained to determine the radius of the trajectory followed by the bead (X_{bead}).*

3.4.3 Worm-like chain fit

The effect of pulling on DNA with and without doxorubucin was then analysed. This was done by fitting a Worm-Like Chain (WLC) model to the force extension data obtained after correcting for the drift and bead offset. The contour length before and after 5μM doxorubucin was analysed to infer the extension of DNA and the number of intercalated doxorubicin molecules.

3.4.4 Extracting the change in linking number

To analyse the relationship between the extension of bare DNA and the change in linking number (ΔLk), a Python code was made which loops through each rotation file for a given force (the force was taken to be F= 0.3 pN) and reads out the relevant data including the position in the z direction for multiple beads attached to DNA. After correcting for the drift, plots of extension (in μ) on the y-axis against the change in linking number on the x-axis were then made.

A moving mean was then calculated, and the top 5% of the y-values of the moving mean were determined. Averaging these values out results in the y-coordinate of the peak of the curves, ie. the measured maximum extension of each bead (h_m in Figure 3.4), which was corrected for the attachment of the DNA relative to the bead z_bead according to equation 3.2. The corresponding x-value ie. the change in linking number of rotationally unstressed DNA (ΔLk_o) was also determined and was similarly stored in an array. Data from multiple files was then combined and analysed and histograms of ΔLk_o at F = 0.3 pN before and after doxorubicin were obtained.

3.4.5 Fitting model for chromatin fiber analysis

The reconstituted chromatin fibres were analysed using a statistical mechanics model formulated by Meng et al. (2015) which allowed us to determine values for the number of nucleosome and tetrasomes in our sample from their force-extension curves [27].

Chapter 4

Results

4.1 The mechanical properties of DNA change upon addition of doxorubicin

Figure 4.1 shows a force-extension curve for the same DNA molecule without doxorubicin (marked in blue) and with doxorubicin (marked in red). The measurement with doxorubicin was taken following a 10 minute incubation period.

A WLC model was fit to the bare DNA strand with fixed contour length of 4531 bp. This yielded a persistence length of 62.03 $\pm$ 2.40 nm which is slightly higher than the literature values for the persistence length of bare DNA, reported to be between 45 and 55 nm [28] [15]. Additionally, z_{bead} was fitted, which yielded 0.8μm, indicating that the DNA was attached about half way the bottom hemisphere of the bead.

At higher forces, the extension approaches the contour length according to the WLC model, and for forces between 55 and 60 pN, the measured extension for the DNA shown in Figure 4.1 is 1.53 $\pm$ 0.01 μm in the absence of doxorubicin. This increases to 2.38 $\pm$ 0.04 μm after the addition of 5 μM doxorubicin, giving an extension of 850 nm. Given that each doxorubicin molecule causes an extension of 0.34 nm (due to intercalation), it implies that approximately 2500 doxorubicin molecules are intercalated into a DNA strand of 4.5 kbp.

After doxorubicin addition, the contour length (L) increases due to the doxorubicin molecules intercalating between base pairs. This may also

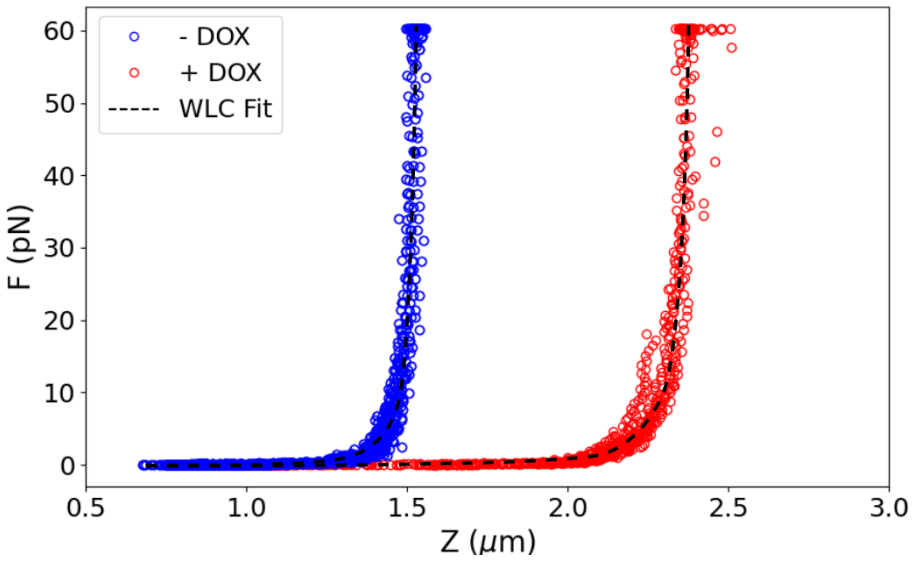

Figure 4.1: 5 μM doxorubucin increased the contour length of DNA *DNA before doxorubucin addition (blue data points) had a contour length of 4531 bp, which increases to 7673 ± 27 bp after doxorubucin addition (red data points) according to the WLC model fit (black dashed lines).*

cause a change in A. The value for z_{bead}, however, remains unchanged with doxorubicin addition. Consequently, for the curve with doxorubicin we fitted L and A, while fixing z_{bead} to the previously obtained value. The WLC fit yielded L = 7673 $\pm$ 27 bp and A = 44.10 $\pm$ 1.22 nm. The results show that doxorubicin intercalation, causes an increase in the contour length of DNA. Meanwhile, the persistence length decreased from the fitted value in the absence of doxorubicin and could indicate that the DNA became more flexible after doxorubicin.

4.2 Doxorubicin's effect on extension and linking number

When DNA is rotated, plectonemes form, causing the end-to-end distance of the DNA to decrease, resulting in smaller extensions as the number of rotations increases. As DNA is twisted, the linking number of the DNA strand also changes. This behavior is illustrated in Figures 4.2 (a) and 4.2 (b), which show graphs of DNA extension in the z direction against the change in DNA linking number (ΔLk).

Without doxorubicin (Figure 4.2 (a)), the graphs are symmetric at forces of 0.7 pN and below, indicating that the direction of magnet rotation does not significantly impact plectoneme formation. However, as the force increases, asymmetry is introduced. The extension versus ΔLk at different forces show maximum extension when ΔLk is 0. This is expected since, at 0 rotations, there are no supercoils in the DNA strand, resulting in the DNA being at its longest. As the force increases, the overall extension of the DNA also increases due to the stretching of the DNA following the WLC model, leading to greater length at 0 twists.

Figure 4.2 (b) shows curves of extension versus change in linking number for different forces on the same DNA strand depicted in Figure 4.2 (a), upon addition of doxorubicin. From the graph, it is evident that two changes occur: first, the curves shift to the left, and second, the overall extension of the DNA strand increases. For a force of 0.3 pN, the extension increases from 0.98 μm (before doxorubicin) to 1.11 μm (after doxorubicin), while the peak shifts from 0.22 turns in rotation (before doxorubicin) to -39.95 turns (after doxorubicin). This shift towards negative twist agrees with literature and shows that doxorubicin caused DNA to untwist.

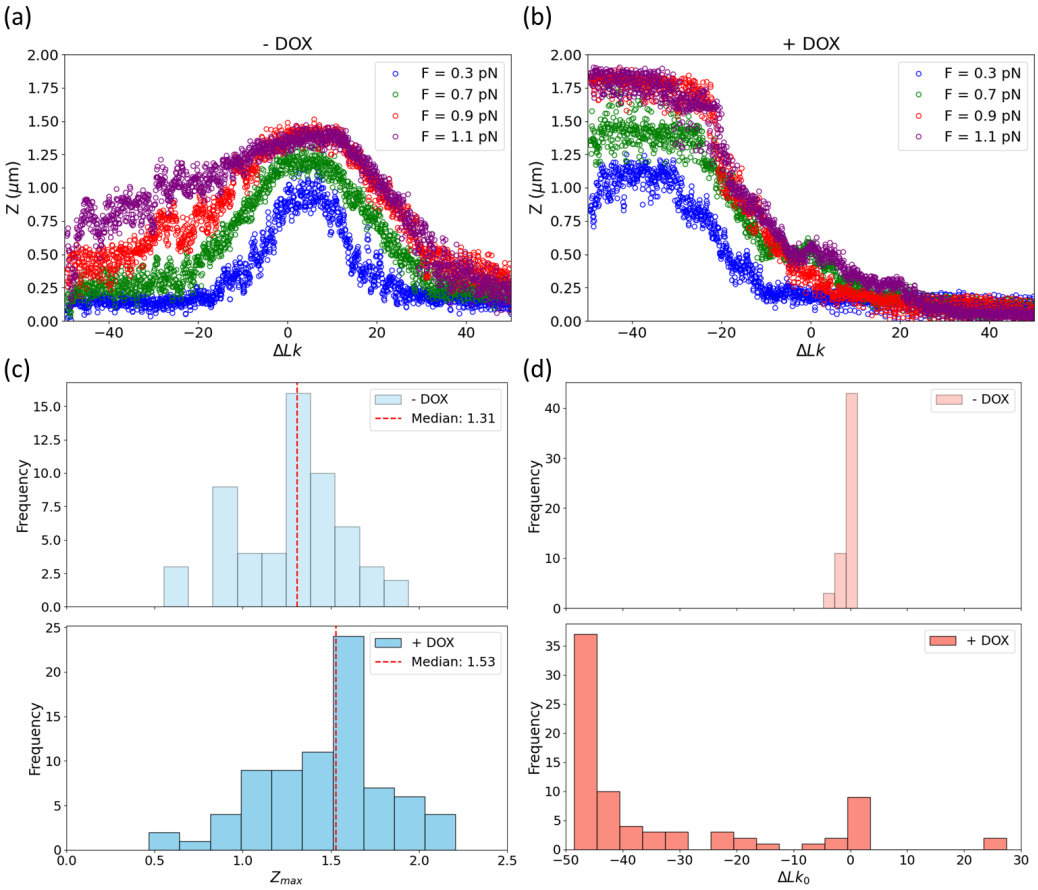

Figure 4.2: Doxorubucin addition causes an increase in DNA extension and a change in linking number *Curves (a) and (b) show a strand of DNA undergoing rotations at different forces before and after adding 5 μM doxorubicin respectively. The data points are colored blue for a force F = 0.3 pN, green for F = 0.7 pN, red for F = 0.3 pN, and purple for F = 1.1 pN. Higher extensions are observed after adding doxorubicin across all forces. A shift towards negative linking number values are also observed indicating untwisting of DNA due to doxorubicin intercalation. (c) Histograms of maximum extension (z_{max}) without doxorubicin (top) and with doxorubicin (bottom) for F = 0.3pN showing an increase in extension of 220nm. (d) Histograms of change in linking number of non-stressed DNA (ΔLk_o) without doxorubicin (top) and with doxorubicin (bottom) for F = 0.3pN showing shift towards negative values of ΔLk_o in the latter case. The same data set was used to obtain histograms (c) and (d) with a sample size of 57 DNA strands without doxorubicin and 77 DNA strands with doxorubicin.*

For a force of 0.3 pN, the maximum extension (Z_{max}) was determined for 57 DNA strands before the addition of doxorubicin and 77 DNA strands after the addition of doxorubicin. Histograms showing the overall distribution were then plotted in Figure 4.2(c). The maximum extensions were corrected for the attachment of the DNA relative to the bead according to equation 3.2.

The maximum extension varied between 0.55 μm to 1.94 μm before adding doxorubicin, and from 0.47 μm to 2.21 μm after adding doxorubicin. Additionally, there is an overall shift towards higher extensions after the addition of doxorubicin. Before doxorubicin addition, the distribution had a median extension of 1.31 μm and a mean of 1.27 $\pm$ 0.29 μm. After doxorubicin addition, the median extension increases to 1.52 μm and the mean to 1.46 $\pm$ 0.35 μm.

For the same data set a histogram of the change in linking number for non-stressed DNA (ΔLk_o) was plotted (Figure 4.2(d)). This value is directly proportional to the number of doxorubicin molecules intercalated in the DNA strand (equation 2.5). A shift to negative values of ΔLk_o after doxorubucin addition is seen. Before adding doxorubicin, ΔLk_o ranged around a median value of -0.02, while mean ΔLk_o was -0.58 $\pm$ 1.12, showing that there is little change in the linking number of DNA strands in the absence of doxorubicin. After adding doxorubicin, this range shifts significantly, with the distribution having a median of -43.33 and a mean of -33.55 $\pm$ 19.41. Following doxorubicin addition, the distribution becomes wider as the variability in data increased.

The shift towards negative values of ΔLk_o in the presence of 5 μM doxorubicin can be explained by the intercalation of the molecule between DNA base pairs, which causes the DNA strand to untwist and reduces the linking number of the DNA. From a sample size of 77, the majority (74%) of the DNA strands show a value of ΔLk_o of -28 or less. Interestingly, a fraction of the curve (14%) show little to no shift.

One possible explanation for this could be heterogeneity in our sample, where some DNA strands acquire more doxorubicin intercalations than others. Another more likely possible explanation could be that DNA strands showing little to no changes in twist are situated at the edge of the flow cell, where the magnetic field is less strong, allowing these DNA strands to relax and return to their optimal linking number. From the 77,

two clear outliers have a positive ΔLk_o of around 25 turns which is unexpected given the known intercalative action of doxorubicin.

4.3 Doxorubicin causes nucleosome dissociation

Chromatin was reconstituted from bare DNA as explained in Section 3.2. This reconstituted chromatin was then assessed using agarose gel electrophoresis, and the results are shown in Figure 4.3.

The bare DNA sample, which contains only DNA without histones, migrated as a single band at a position corresponding to its contour length of 3 kbp (Figure 4.3). Additionally, a much fainter band was observed higher up in the gel, likely representing uncut plasmid DNA that remained undigested. The chromatin reconstitutions exhibited slower migration than the bare DNA sample. As the histone concentration increased, the migration decreased until saturation was reached. Beyond this point, excessively high histone concentrations resulted in suboptimal reconstitutions, affecting the migration pattern.

Chromatin with a DNA:histone molar ratio of 1:0.9 showed a broadened band, suggesting an insufficient number of histones to fully fold the DNA. In contrast, chromatin with DNA:histone molar ratios of 1:1.4 and 1:1.9 exhibited the sharpest bands, showing optimal chromatin formation. At a DNA:histone ratio of 1:2.4 a relatively small and faint band appears, with some material remaining in the well, suggesting oversaturation with histones. Thus the optimal DNA: histone molar ratio in this experiment was 1:1.9, and this ratio was used in the subsequent magnetic tweezer experiments.

To investigate the effect of doxorubicin on our reconstituted chromatin samples, we conducted a second gel electrophoresis experiment. In this experiment, we compared the four chromatin reconstitutions with and without 5 μM doxorubicin (Figure 4.4).

The bare DNA showed a sharp band both before and after doxorubucin addition. In contrast, the chromatin samples exhibited a transition from sharp bands to more diffuse and fuzzy bands after incubation with 5 μM doxorubucin. Additionally, a thin band of bare DNA became more prominent in the chromatin samples post-doxorubicin addition.

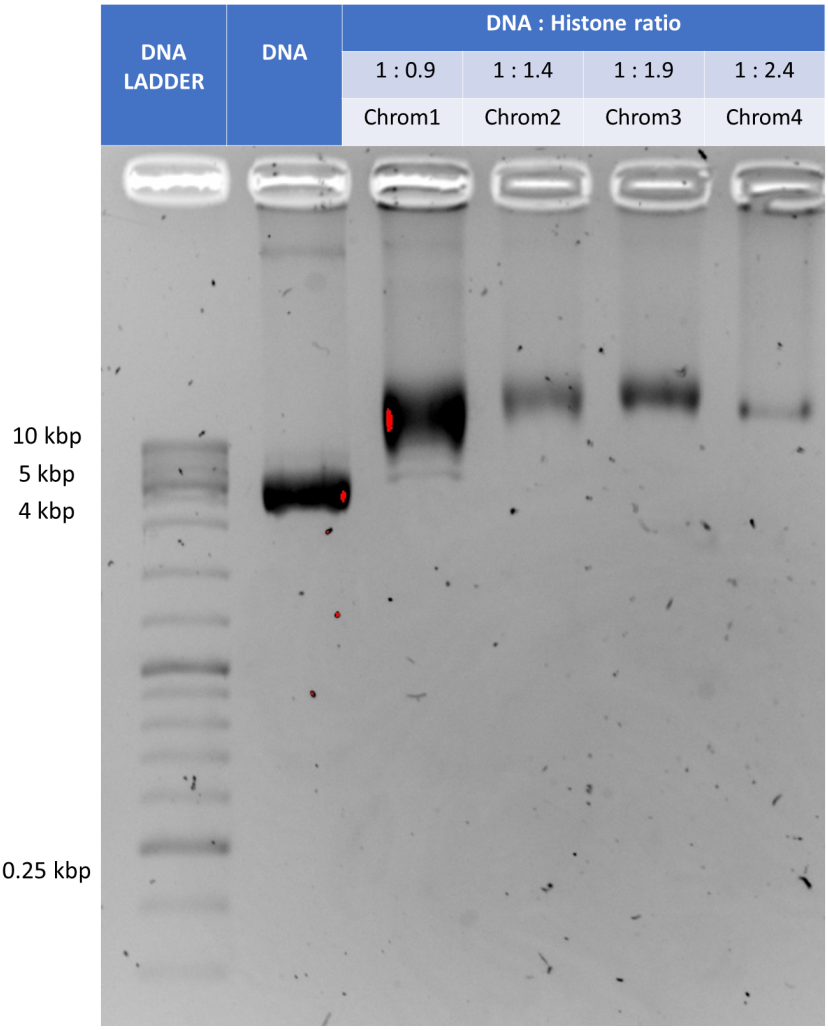

Figure 4.3: Agarose gel electrophoresis results showing chromatin reconstitutions using different DNA:histone ratios. *Chromatin was reconstituted with 4 different DNA:histone molar ratios (1:0.9, 1:1.4, 1:1.9 and 1:2.4) by using salt dialysis. Ladder and bare DNA were placed in well 1 and well 2 respectively for comparison. Chromatin reconstitutions show slower migration the higher the histone content. Chrom1 had the least histone content and displays a fuzzy band indicating an insufficient number of histones to fully fold the DNA. While Chrom4 had the highest histone content and shows signs of saturation.*

The larger, more spread-out bands observed in the chromatin samples after doxorubicin addition could imply that histones were expelled from the chromatin. This is consistent with the hypothesis that doxorubicin induces chromatin destabilization, causing histone dissociation and the creation of more bare DNA.

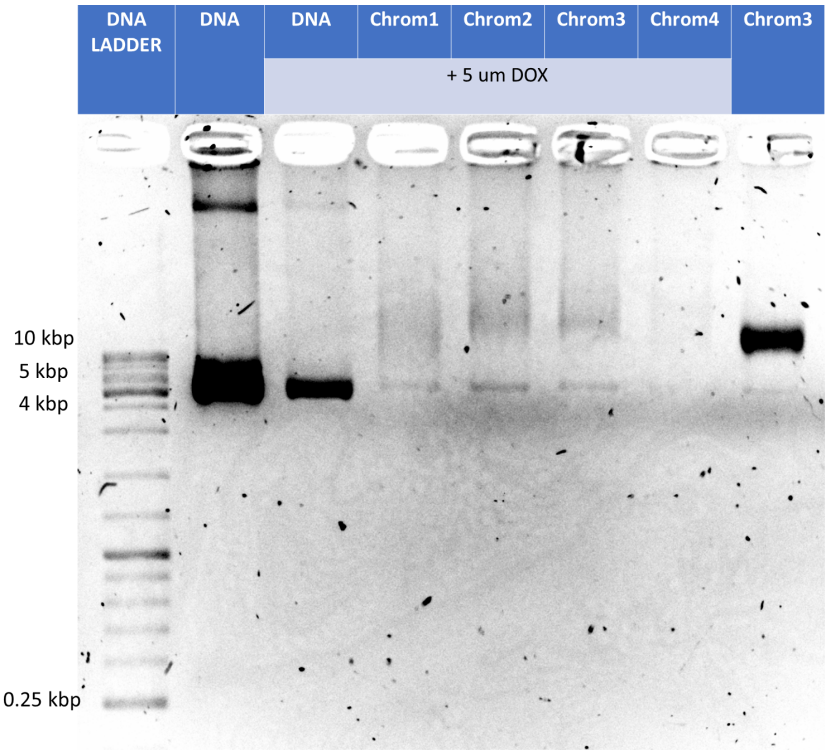

Figure 4.4: Agarose gel electrophoresis showing chromatin dissociation after addition of 5 μM doxorubicin. *The wells show DNA ladder, bare DNA, DNA and the four reconstituted chromatins having DNA:histone molar ratios or 1:0.9, 1:1.4, 1:1.9 and 1:2.4 (marked as Chrom1, Chrom2, Chrom3 and Chrom4 respectively) with 5 μM doxorubicin. The last well contains only chromatin having DNA:histone molar ratio 1:1.9 for comparison. The bare DNA and chromatin samples were premixed with Doxorubicin in tubes and allowed to incubate for 10 minutes. All samples were then stained with Safe Red dye, added to the wells and run through the agarose gel at 150 V. Image contrast was heightened for visual interpretation of results*

4.4 Force-extension analysis of chromatin

Figure 4.5 (a) shows the behavior of a chromatin fiber pulled up to a force of 8 pN (blue data points). This fiber was then released, pulled and released again at the same force and for the same duration (grey data points). A plateau is observed at a force of approximately 3 pN, indicating a gain in extension as nucleosomes are unwrapped. Figure 4.5 (b) presents a force-extension curve for a chromatin fiber pulled up to a force of 60 pN. The blue data points represent two subsequent pulling events, while the grey data points show their release. In both low-force and high-force pulling experiments, the curves indicate the destructiveness of the pulling process, as the chromatin structure does not reassemble itself, resulting in hysteresis behavior.

The effect of pulling on chromatin at forces above 10 pN is irreversible, and the chromatin fiber (Figure 4.5 (b)) behaves like a worm-like chain (WLC) when pulled a second time showing the total dissociation of all nucleotides present and the transition to bare DNA. For forces below 10 pN (Figure 4.5(a)), the process should be reversible; however, although there is some overlap between the second pulling curve and the first, hysteresis is observed at low force.

Fits for both curves were made using a statistical mechanics model developed by Meng et al. [27]. This model allowed us to determine the number of nucleosomes in our chromatin fibers as well as the energies involved. In both chromatin fibers shown, the number of nucleosomes is 6, while the number of tetrasomes, ie singly wrapped nucleosomes, is 2. Given that the chromatin used contains 16 repetitions of 601 fragments, the expected number of nucleosomes is 16. This discrepancy suggests that partial nucleosome dissociation happened to the chromatin between reconstitution and its measurement in the magnetic tweezers.

It is likely that during tether assembly, the flow rate, was too high, causing the fibers to partially disassemble between reconstitution and the pulling experiment. The process of flushing fluid through the channels in the flow cell is critical, as the drag on the bead creates a force on the tether, which can disrupt the chromatin structure.

For a series of 5 chromatin fibres, the fit yielded values for the energies involved. The stacking energy (ΔG_1) ranged from 15 kT to 47 kT, and the unwrapping energy (ΔG_2) describing the energy transition from structure

II to structure III (2.4) had values from 5 kT to 26 kT.

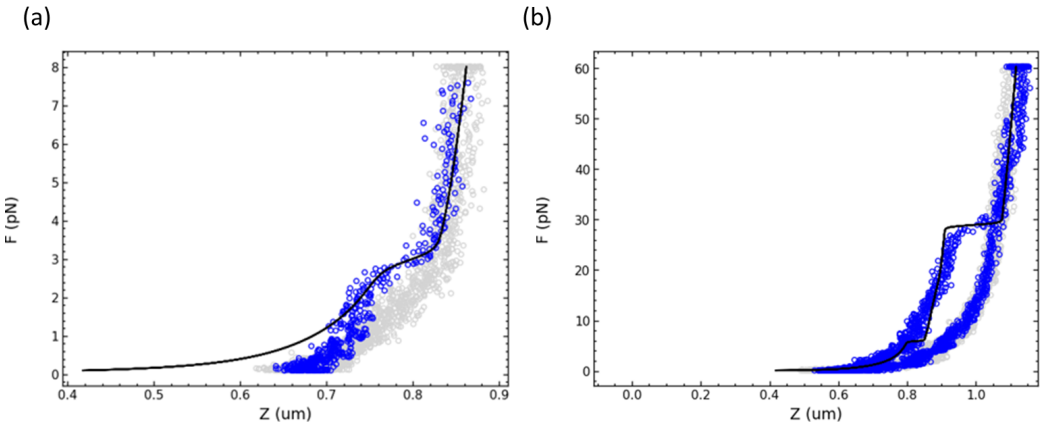

Figure 4.5: Force extension graphs for chromatin *(a) Pulling of chromatin up to a force of 8 pN shows a plateau at around 3 pN indicating nucleosome unwrapping. Blue data points represent a single pulling event, while grey data points show a subsequent release, followed by another pulling event and release. (b) Pulling up to 60 pN for complete dissociation of all histones in the chromatin fibre. Both (a) and (b) demonstrate hysteresis behavior, where subsequent pulling does not follow the same force-extension curve as the initial pulling. Model fitting to the data indicates that the chromatin fiber contains 6 nucleosomes and 2 tetrasomes.*

Chapter 5

Discussion

The mechanical properties of DNA undergo significant changes upon the addition of 5 μM doxorubicin. Fitting the worm-like chain (WLC) to force-extension curves showed that doxorubicin intercalation increased the contour length of DNA from 4531 bp to 7673 $\pm$ 27 bp. The extension at forces between 55 and 60 pN increased by 850 nm after doxorubicin addition, implying the intercalation of approximately 2500 doxorubicin molecules. In rotational experiments, doxorubicin caused a negative shift in the DNA extension versus linking number curves and the change in linking number (ΔLk) after doxorubicin was measured to be -33.55 $\pm$ 19.41, indicating untwisting. Additionally, our agarose gel electrophoresis results show that doxorubicin disrupts chromatin structure and causes histone dissociation.

For a contour length of 4531 bp and the persistence length of 50 nm for bare DNA, the worm-like chain (WLC) model predicts an extension of 1.12 μm at a force of 0.3 pN, which is within the range of our extension obtained of 1.27 $\pm$ 0.29 μm. Assuming the measured 2500 doxorubicin molecules intercalated and using the literature value that each doxorubicin molecule causes an extension of 0.34 nm, the new contour length after adding doxorubicin can be determined and used to plot a WLC curve and determine the expected extension at F = 0.3 pN [29]. For this new L, an extension of 1.77 μm should be observed, which is also within range of the extension obtained of 1.46 $\pm$ 0.35 μm during this research project.

The fitted persistence length of 62.03 $\pm$ 2.40 nm for bare DNA without doxorubicin decreased to 44.10 $\pm$ 1.22 nm after doxorubicin addition. An optical tweezers study conducted by Silva et al. (2016) report a non-monotonic behaviour of the persistence length of DNA depending on the

drug concentration as well as the range in forces used [30]. Typically intercalating drugs are observed to cause an increase in the persistence length as the stacking of the hydrophobic molecules stabilise the DNA, and increases its stiffnes. However the range in pulling forces used still plays a significant role and could have led to a partial melting of the significantly altered double-helix structure of DNA after doxorubicin addition. As shown through the shift towards negative linking numbers from -0.58 $\pm$ 1.12 to -33.55 $\pm$ 19.41 following addition of 5 μM doxorubicin, DNA untwists significantly after the drug's intercalation. This could distort the hydrogen bonds surrounding the binding site and cause the observed decrease in persistence length [31].

Additionally, our measurement of the average change in linking number of unstressed DNA (ΔLk_o) to a value of -33.55 $\pm$ 19.41 using magnetic tweezers is within the range of the -41 value reported by Salerno et al. (2020) [32]. Assuming 2500 doxorubicin molecules and using our median ΔLk_o value of -43.33, we calculate an untwisting angle of approximately -6° per intercalated doxorubicin molecule. This value is notably lower than the range of values reported in the literature, which vary from -11° to -27° per molecule [33] [32]. However, the discrepancy between our results and the published values could be due to the uncertainty in the exact number of doxorubicin molecules intercalated into the DNA which could indeed be lower than the assumed value of 2500.

In the case of chromatin fibres, native gel electrophoresis results show that doxorubicin causes histone expulsion and the dissociation of chromatin fibres. This finding is consistent with previous studies that also demonstrate doxorubicin inducing histone eviction [34] [35]. The action of doxorubicin as an intercalating agent into DNA and displacing histones may be relevant for its effectiveness as an anti-cancer drug. By unwinding DNA and disrupting chromatin structure, doxorubicin effectively hinders DNA replication and transcription, leading to apoptosis in rapidly dividing cancer cells.

Furthermore, a significant decrease in intensity was observed in all gel electrophoresis bands containing doxorubicin. The reduced band intensity seems to suggest that the Safe Red dye, which was used to stain the DNA and chromatin samples, competes with doxorubicin. While doxorubicin is an intercalating agent that inserts itself between DNA base pairs, Safe Red binds to DNA through minor groove binding. Doxorubicin's intercalation could affect the DNA structure, such that the minor groove is

affected hence reducing the binding efficiency of Safe Red.

5.1 Limitations and possible improvements

One main issue encountered during the experiments was the sticking of superparamagnetic beads to the surface, resulting in a smaller dataset. This problem could potentially be adressed by changing the method of assembling the flow cells. For instance, using polyacrylamide gel to anchor the DNA to the glass slide might prevent bead adhesion and improve data collection.

Due to time constraints, measurements for pulling DNA before and after doxorubicin addition were not performed on the same DNA strands. Instead, different regions of interest were used, leading to inconsistent determination of the z_{bead} across pulling measurements. This introduced variability in the data that could have been minimized by using the same DNA strands throughout the experiments. Future work should involve performing pulling experiments on a larger number of data points before and after doxorubicin addition. This would provide a better supported conclusion on the exact changes in contour length and persistence length.

While correcting for the offset due to bead attachment z_{bead}, it was noted that all values of z_{bead} were smaller than 0.9 μm, resulting in no significant change in the extensions before and after accounting for this offset. This was due to the contour length of the DNA being comparable to the radius of the bead, causing larger z_{bead} values to lead to bead adhesion to the bottom of the flow cell. One improvement could hence be to utilise smaller beads or alternatively longer DNA strands.

Lastly, throughout this research project, chromatin pulling measurements before and after doxorubicin addition were not performed. Conducting these measurements in future studies would be beneficial as they would allow for the direct observation of the exact effect of doxorubicin on chromatin structure, including the number of nucleosome dissociations that occur. This could provide valuable insights into the mechanisms by which doxorubicin exerts its effects on chromatin.

Chapter 6

Conclusion

The mechanical properties of DNA were investigated under the influence of clinically relevant concentrations of the chemotherapy drug doxorubicin. Our study showed that doxorubicin increases the contour length of DNA and induces a shift in the linking number towards negative values, consistent with prior research highlighting its action in untwisting DNA. This change in DNA's mechanical behavior destabilizes nucleosomes, as evidenced by histone dissociation observed in all chromatin samples treated with doxorubicin during gel electrophoresis.

Our findings underscore the importance of understanding the precise mechanisms through which doxorubicin disrupts chromatin structure. Future investigations should focus on quantifying the relationship between changes in DNA twist and extension and the dissociation of nucleosomes within chromatin fibers. Expanding upon this study could involve exploring the molecular mechanisms of doxorubicin and its variants, aiming to enhance the therapeutic index, minimize damage to healthy cells, and maximize the impact on cancerous ones.

In conclusion, this research highlights the necessity of studying drug-DNA interactions at the molecular level. By elucidating how doxorubicin modifies DNA and chromatin structure, we contribute to advancing scientific understanding and pave the way for the development of improved chemotherapeutic agents tailored to more effectively target cancer cells.

Version of June 25, 2024– Created June 25, 2024 - 10:33

Bibliography

[1] C. F. Thorn, C. Oshiro, S. Marsh, T. Hernandez-Boussard, H. McLeod, T. E. Klein, and R. B. Altman, *Doxorubicin pathways: pharmacodynamics and adverse effects*, Pharmacogenet Genomics **21**, 440 (2011).

[2] Y. Pommier, E. Leo, H. Zhang, and C. Marchand, *DNA Topoisomerases and Their Poisoning by Anticancer and Antibacterial Drugs*, Chemistry Biology **17**, 421 (2010).

[3] R. Bosire, L. Fadel, G. Mocsár, P. Nánási, Jr, P. Sen, A. K. Sharma, M. U. Naseem, A. Kovács, J. Kugel, G. Kroemer, G. Vámosi, and G. Szabó, *Doxorubicin impacts chromatin binding of HMGB1, Histone H1 and retinoic acid receptor*, Sci Rep **12**, 8087 (2022).

[4] A. Revyakin, C. Liu, R. H. Ebright, and T. R. Strick, *Abortive initiation and productive initiation by RNA polymerase involve DNA scrunching*, Science **314**, 1139 (2006).

[5] B. Alberts, A. Johnson, J. Lewis, M. Raff, K. Roberts, and P. Walter, *The structure and function of DNA*, Garland Science, London, England, 2002.

[6] J. Bednar, R. A. Horowitz, S. A. Grigoryev, L. M. Carruthers, J. C. Hansen, A. J. Koster, and C. L. Woodcock, *Nucleosomes, linker DNA, and linker histone form a unique structural motif that directs the higher-order folding and compaction of chromatin*, Proceedings of the National Academy of Sciences **95**, 14173 (1998).

[7] W. Fischle, Y. Wang, and C. D. Allis, *Histone and chromatin cross-talk*, Current Opinion in Cell Biology **15**, 172 (2003).

[8] P. Sehgal and P. Chaturvedi, *Chromatin and Cancer: Implications of Disrupted Chromatin Organization in Tumorigenesis and Its Diversification*, Cancers (Basel) **15** (2023).

[9] C. Muller, E. Chatelut, V. Gualano, M. De Forni, F. Huguet, M. Attal, P. Canal, and G. Laurent, *Cellular pharmacokinetics of doxorubicin in patients with chronic lymphocytic leukemia: comparison of bolus administration and continuous infusion*, Cancer Chemotherapy and Pharmacology **32**, 379 (1993).

[10] R. E. Nicoletto and C. M. Ofner, 3rd, *Cytotoxic mechanisms of doxorubicin at clinically relevant concentrations in breast cancer cells*, Cancer Chemother Pharmacol **89**, 285 (2022).

[11] M. Kruithof, F. Chien, M. de Jager, and J. van Noort, *Subpiconewton dynamic force spectroscopy using magnetic tweezers*, Biophys J **94**, 2343 (2007).

[12] C. Bustamante, Z. Bryant, and S. Smith, *Ten years of Tension: Single-molecule DNA mechanics*, Nature **421**, 423 (2003).

[13] M. Lee, J. Lipfert, O. Ordu, J. W. J. Kerssemakers, and N. H. Dekker, *Magnetic Tweezers for the Measurement of Twist and Torque*, JoVE , e51503 (2014).

[14] M. Rubinstein and R. Colby, *Polymer Physics*, Oxford University Press, 2003.

[15] J. Bednar, P. Furrer, V. Katritch, A. Stasiak, J. Dubochet, and A. Stasiak, *Determination of DNA Persistence Length by Cryo-electron Microscopy. Separation of the Static and Dynamic Contributions to the Apparent Persistence Length of DNA*, Journal of Molecular Biology **254**, 579 (1995).

[16] J. F. Marko and E. D. Siggia, *Statistical mechanics of supercoiled DNA*, Phys. Rev. E **52**, 2912 (1995).

[17] J. Segura, R. S. Joshi, O. Díaz-Ingelmo, A. Valdés, S. Dyson, B. Martínez-García, and J. Roca, *Intracellular nucleosomes constrain a DNA linking number difference of â1.26 that reconciles the Lk paradox*, Nature Communications **9**, 3989 (2018).

[18] M. Bansal, *DNA structure: Revisiting the Watson-Crick double helix*, Current Science **85**, 1556 (2003).

[19] W. Gion and D. Adams, *Analysis of Matrix Attachment Region in an Experimental Vector, pA205*.

[20] R. Sarkar and V. V. Rybenkov, *A Guide to Magnetic Tweezers and Their Applications*, Frontiers in Physics **4** (2016).

[21] A. Klug and L. C. Lutter, *The helical periodicity of DNA on the nucleosome*, Nucleic Acids Res **9**, 4267 (1981).

[22] A. Celedon, D. Wirtz, and S. Sun, *Torsional Mechanics of DNA Are Regulated by Small-Molecule Intercalation*, The Journal of Physical Chemistry B **114**, 16929 (2010), PMID: 21090816.

[23] B. Feng, R. P. Sosa, A. K. F. Martensson, K. Jiang, A. Tong, K. D. Dorfman, M. Takahashi, P. Lincoln, C. J. Bustamante, F. Westerlund, and B. Norden, *Hydrophobic catalysis and a potential biological role of DNA unstacking induced by environment effects*, Proceedings of the National Academy of Sciences **116**, 17169 (2019).

[24] D. A. Beshnova, A. G. Cherstvy, Y. Vainshtein, and V. B. Teif, *Regulation of the nucleosome repeat length in vivo by the DNA sequence, protein concentrations and long-range interactions*, PLoS Comput Biol **10**, e1003698 (2014).

[25] T. Brouwer, C. Pham, A. Kaczmarczyk, W.-J. de Voogd, M. Botto, P. Vizjak, F. Mueller-Planitz, and J. van Noort, *A critical role for linker DNA in higher-order folding of chromatin fibers*, Nucleic Acids Research **49**, 2537 (2021).

[26] A. Kaczmarczyk, T. B. Brouwer, C. Pham, N. H. Dekker, and J. van Noort, *Probing Chromatin Structure with Magnetic Tweezers*, pages 297–323, Springer New York, New York, NY, 2018.

[27] H. Meng, K. Andresen, and J. vanÂ Noort, *Quantitative analysis of single-molecule force spectroscopy on folded chromatin fibers*, Nucleic Acids Research **43**, 3578 (2015).

[28] J. P. Peters and L. J. Maher, *DNA curvature and flexibility in vitro and in vivo*, Quarterly Reviews of Biophysics **43**, 23â63 (2010).

[29] J. E. Coury, L. McFail-Isom, L. D. Williams, and L. A. Bottomley, *A novel assay for drug-DNA binding mode, affinity, and exclusion number: scanning force microscopy*, Proc Natl Acad Sci U S A **93**, 12283 (1996).

[30] E. Silva, R. Falchetto Bazoni, E. Bessa Ramos, and M. Rocha, *DNA-doxorubicin interaction: New insights and peculiarities*, Biopolymers **107** (2016).

[31] A. K. Dasanna, N. Destainville, J. Palmeri, and M. Manghi, *Slow closure of denaturation bubbles in DNA: Twist matters*, Phys. Rev. E **87**, 052703 (2013).

[32] D. Salerno, D. Brogioli, V. Cassina, D. Turchi, G. L. Beretta, D. Seruggia, R. Ziano, F. Zunino, and F. Mantegazza, *Magnetic tweezers measurements of the nanomechanical properties of DNA in the presence of drugs*, Nucleic Acids Res **38**, 7089 (2010).

[33] F. Yang, S. S. Teves, C. J. Kemp, and S. Henikoff, *Doxorubicin, DNA torsion, and chromatin dynamics*, Biochim Biophys Acta **1845**, 84 (2013).

[34] B. Pang, X. Qiao, L. Janssen, A. Velds, T. Groothuis, R. Kerkhoven, M. Nieuwland, H. Ovaa, S. Rottenberg, O. van Tellingen, J. Janssen, P. Huijgens, W. Zwart, and J. Neefjes, *Drug-induced histone eviction from open chromatin contributes to the chemotherapeutic effects of doxorubicin*, Nature Communications **4**, 1908 (2013).

[35] S. Y. van der Zanden, X. Qiao, and J. Neefjes, *New insights into the activities and toxicities of the old anticancer drug doxorubicin*, FEBS J **288**, 6095 (2020).

Acknowledgements

I would like to express my deepest gratitude to my supervisor, prof. dr. John van Noort, without whose constant support, guidance and belief in my abilities I would not have been able to present the work I'm presenting today. I am also thankful to our dedicated lab technician, Dr. Maidina Tohti, for her kindness, invaluable assistance in equipment operation, and providing essential protocols.

Additionally, I extend heartfelt thanks to my family. To my parents, my sister, and aunt Maria. Your constant love, encouragement, and support have been essential for my academic journey. To my friends here, who have become like family, your support and companionship have made this endeavor possible and meaningful.

This research project marks the completion of my MSc Physics studies, and I am grateful for the collective support that has enriched my academic and personal growth.

Chapter 7

Supplemental Data

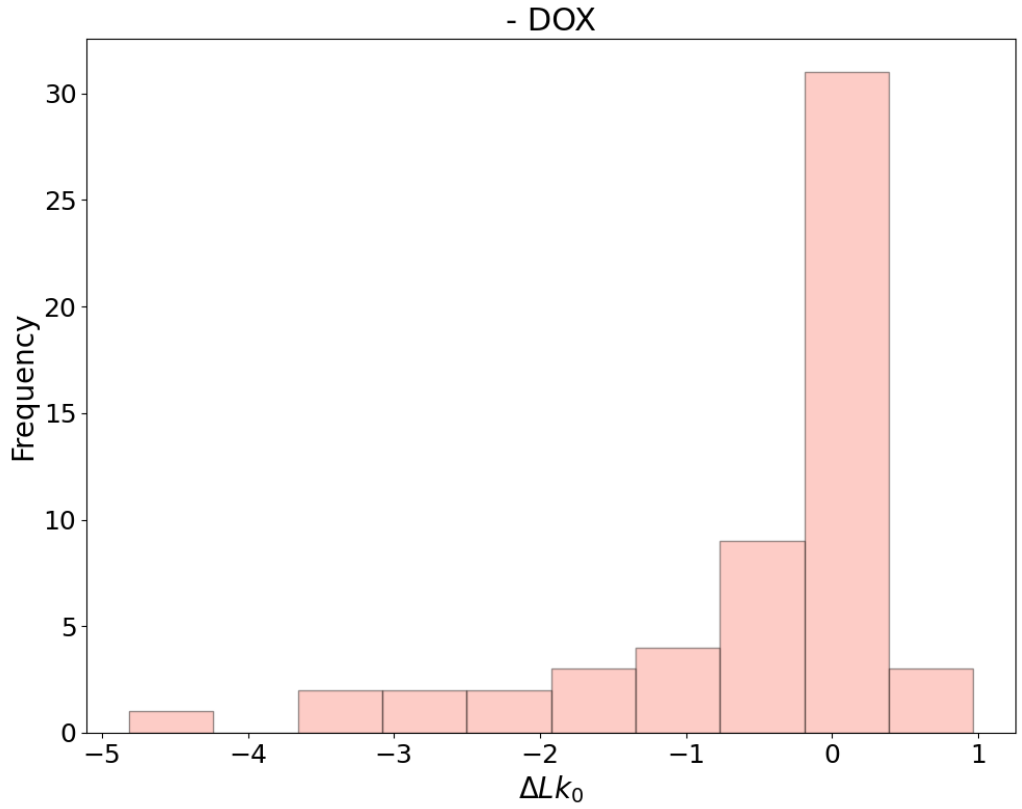

Supplementary Figure 7.1: ΔLk_o ***distributed around 0 for DNA strands in the absence of Doxorubucin*** *Histogram shows of the distribution in* ΔLk_o *for a sample of 57 DNA strands without doxorubicin at a force F = 0.3 pN. Bin width = 0.578 and mean* ΔLk_o *= -0.58* $\pm$ *1.12*

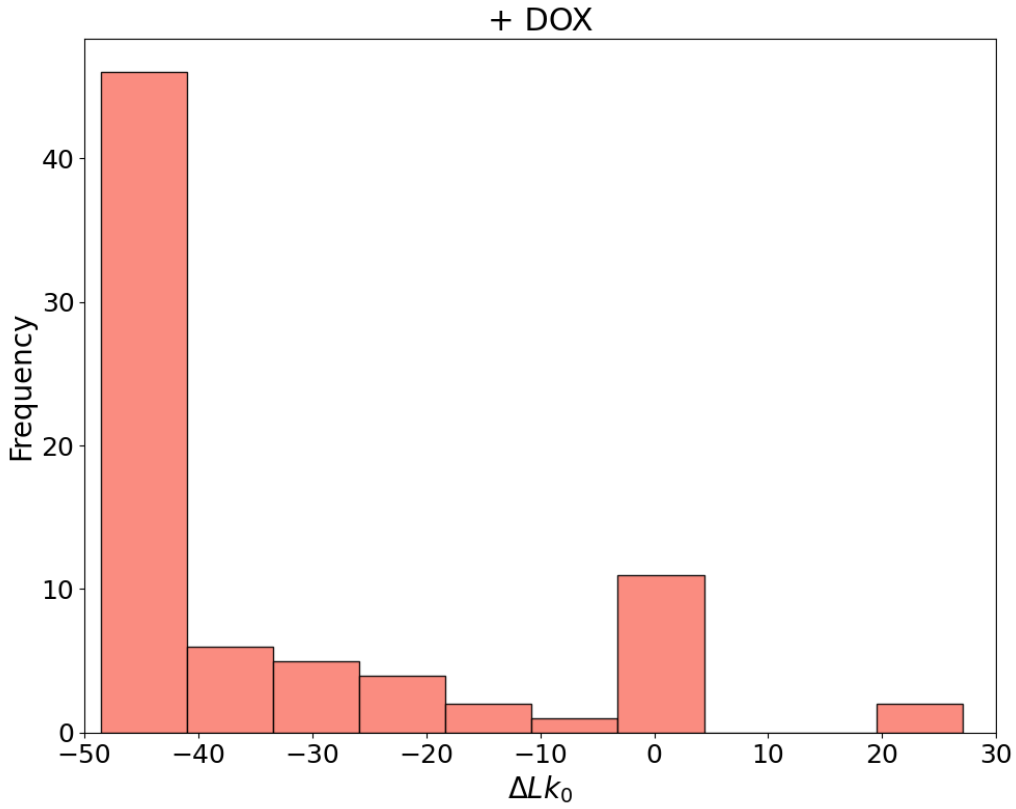

Supplementary Figure 7.2: Negative shift in ΔLk_o ***observed for DNA strands in the absence of Doxorubucin*** *Histogram shows of the distribution in* ΔLk_o *for a sample of 77 DNA strands with 5* μ*M doxorubicin at a force F = 0.3 pN. Bin width = 7.56 and mean* ΔLk_o *= -33.55* $\pm$ *19.41*

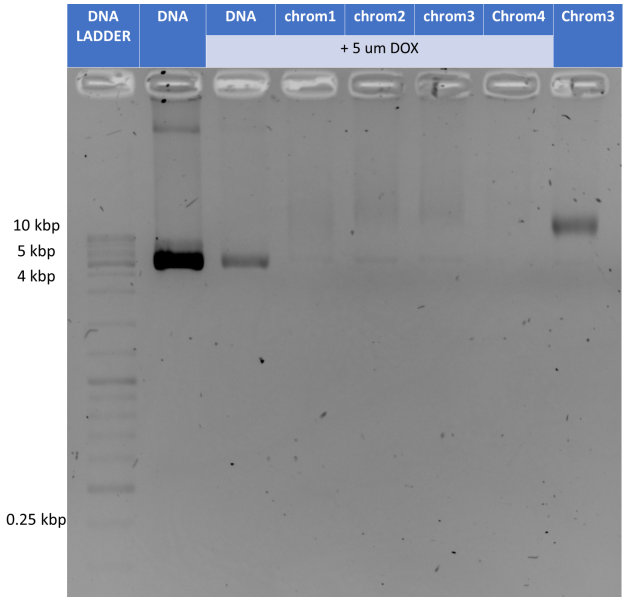

Supplementary Figure 7.3: Agarose gel electrophoresis showing low intensity bands as Safe Red dye competes with doxorubicin *The wells show DNA ladder, bare DNA, DNA and the four reconstituted chromatins having DNA:histone molar ratios or 1:0.9, 1:1.4, 1:1.9 and 1:2.4 (marked as Chrom1, Chrom2, Chrom3 and Chrom4 respectively) with 5 μM doxorubicin. The last well contains only chromatin having DNA:histone molar ratio 1:1.9 for comparison. The bare DNA and chromatin samples were premixed with doxorubicin in tubes and allowed to incubate for 10 minutes. All samples were then stained with Safe Red dye, added to the wells and run through the agarose gel at 150 V. Doxorubicin seems to compete with Safe Red as all bands containing doxorubicin show a significant decrease in intensity*